Alignment and Orientation Effects in Sr Energy Pooling

Harold V. Parks and Stephen R. Leone*

JILA, National Institute of Standards and Technology and University of Colorado, and the Departments of Physics and Chemistry and Biochemistry, University of Colorado, Boulder, Colorado 80309-0440

Received: May 26, 1999; In Final Form: July 7, 1999

Alignment and orientation effects in the energy pooling process, $Sr(5s5p\ ^3P_1) + Sr(5s5p\ ^3P_1) \rightarrow Sr(5s5p\ ^1P_1) + Sr(5s^2\ ^1S_0)$, are studied in a single atomic beam. The Sr atoms are prepared in an aligned initial state with a polarized laser, and alignment information is extracted by observing the fluorescence from the final $Sr(5s5p\ ^1P_1)$ state as the atoms precess in an applied magnetic field. This allows the dependence of the total energy pooling cross section (integrated over the final state alignment) on the initial state alignment to be almost completely described. A prominent alignment effect is observed. If m_j represents the component of total electronic angular momentum of a $Sr(5s5p\ ^3P_1)$ atom along the relative velocity vector of the collision, then the total energy transfer cross section for a particular initial state alignment can be expressed as a sum of the so-called fundamental cross sections, $\sigma_{m_1m_2}$ and $\sigma_{m_1m_2;m_1'm_2'}$, that describe collisions between the various m_j states. Here $\sigma_{m_1m_2}$ represents the cross section for energy transfer when an atom in state m_1 collides with an atom in state m_2. The cross section $\sigma_{m_1m_2;m_1'm_2'}$ represents the contribution to the total cross section from interference when the colliding system is in a superposition of the state m_1 colliding with m_2 and the state m_1' colliding with m_2'. It is found that the cross sections σ_{1-1}, σ_{00}, and σ_{10} as well as the interference terms $\mathrm{Re}(\sigma_{00;1-1})$ and $\sigma_{01;10}$ have relatively large values while σ_{11} and $\sigma_{1-1;-11}$ are small. Coupled with future theoretical work, these results may provide new insights into the dynamics of the curve crossings that lead to energy transfer.

I. Introduction

Vector correlation experiments provide a powerful method for exploring the interaction between atoms or molecules.[1−4] By aligning and orienting the atoms with a laser before a collision, the molecular state of the colliding atoms can be controlled. This gives an exacting probe of the interatomic potentials as well as insight into the collision dynamics. Many two-vector experiments have been done where one of the colliding atoms is aligned with respect to the relative velocity vector of the collision, just a few of which are referenced here.[5−9] Less common are three-vector experiments where two aligned atoms are collided[10−14] or where an aligned atom collides with a structureless atom and the final state alignment is probed.[15−17] Again, the relative velocity vector of the collision is one of the controlled vectors. Most rare are four-vector experiments. These usually involve the initial and final velocity together with initial and final alignments.[15−17] In previous work by this group an experiment has been done where two aligned excited state Ca atoms collide and the final state is resolved.[18]

In this work we study alignment and orientation effects for the process:

$$Sr(5s5p\ ^3P_1) + Sr(5s5p\ ^3P_1) \rightarrow Sr(5s5p\ ^1P_1) + Sr(5s^2\ ^1S_0) \quad (1)$$

This paper concentrates on a three-vector experiment where the effects of initial state alignment on the total energy pooling cross sections are studied, ignoring the final state alignment. However, observations of the final state alignment will be briefly mentioned. Energy pooling of atomic Sr has been extensively studied by Neuman et al.[19] and Kelly et al.[20] Neuman et al. have even briefly examined the initial state alignment dependence of several of these processes, including the process in eq 1.[21] They saw no alignment effects for this particular process, but their technique was less sensitive than ours, and they were not able to explore all possible collision geometries. With our technique, a distinct alignment effect is apparent.

These Sr experiments complement our previous studies of the analogous system in Ca:[18,22]

$$Ca(4s4p\ ^3P_1) + Ca(4s4p\ ^3P_1) \rightarrow Ca(4s4p\ ^1P_1) + Ca(4s^2\ ^1S_0) \quad (2)$$

The outer shell electronic structures of Sr and Ca are remarkably similar, and the Sr alignment effects are reminiscent of the Ca results. However there are also some important differences. Since spin orbit coupling is reasonably strong in both cases, the aligned quantity is the total (spin plus orbital) electronic angular momentum. The initial relative velocity vector of the collision provides a natural quantization axis, and the aligned states will be labeled by the component of angular momentum along this axis, m_j. With both Ca and Sr, collisions between two $m_j = +1$ atoms have a small cross section (here we are averaging over all final magnetic substates), but the relative cross section is higher for Sr than Ca. In Ca the cross section for $m_j = +1$ plus $m_j = 0$ collisions is also small, but it is much more substantial in Sr. In Ca there is an important interference term present when each atom is in a superposition of an $m_j = +1$ and an $m_j = -1$ state, but this seems to play no role in the Sr

* Corresponding author and staff member, Quantum Physics Division, National Institute of Standards and Technology.

10.1021/jp991743d
Published on Web 08/21/1999

case. With both Sr and Ca energy pooling, the $m_j = +1$ plus $m_j = -1$ and $m_j = 0$ plus $m_j = 0$ cross sections are large.

These experiments are carried out in a single atomic beam. The initial Sr(5s5p $^3P_1$) states are prepared with a polarized laser pulse and the fluorescence from the final Sr(5s5p $^1P_1$) state is observed. After the laser pulse the initial state population evolves under the influence of an applied magnetic field. This magnetic field can be constant, causing the entire population of atoms to precess, always maintaining the same alignment with respect to each other, but changing the alignment periodically with respect to the relative velocity vector of the collision. Alternatively, we introduce a magnetic field gradient so that atoms at different positions will precess at different rates so that collisions between atoms with different alignments can be realized.

The apparatus and techniques used in this experiment have already be described in our Ca work,[18,22] so they will only be outlined here. Section II briefly describes the apparatus and section III outlines the mathematical framework that is used to analyze the alignment results. Section IV describes the experiments where the effects of initial state alignment are studied, integrating over all final states. Section V summarizes the observations of final state alignment. The results are discussed and compared to the Ca results in section VI.

II. Experimental Apparatus

The apparatus used for this experiment has been described in detail in Parks et al.[18,22] Only a brief outline is given here. Strontium vapor is produced in an oven held at 910−920 K. The Sr beam emerges from a nozzle that is heated to a slightly higher temperature, 950−960 K, to prevent clogging. These temperatures are slightly lower than those used in the Ca experiments of Parks et al.[18,22] Since the vapor pressure of Sr is higher than Ca, the atomic density produced by the oven is comparable in both cases. With Sr, the density is 6×10^{10} atoms/cm^3 at a distance 6 cm from the nozzle, where the excitation laser intersects the atomic beam. This assures that single collision conditions are attained on the time scale of this experiment.

The atomic beam is excited with 689 nm light from a Nd:YAG pumped pulsed dye laser to produce the initial Sr(5s5p $^3P_1$) state. The laser has a repetition rate of 10 Hz, a pulse width of 5 ns, and a pulse energy of about 1 mJ. If needed, the vertically polarized output of this laser is put through a double Fresnel rhomb to rotate the polarization before it goes through a polarizer to clean up the polarization. If circular polarization is needed the laser beam is then put through a Soleil-Babinet compensator.

The rest of the apparatus is identical to that described in Parks et al.[18,22] After the laser pulse, the initial state Sr atoms precess with a period of 0.8 μs, in a magnetic field produced by a set of Helmholtz coils. Note that the lifetime of the final Sr(5s5p $^1P_1$) state is only a few nanoseconds, so this decay is instantaneous on the time scale of the magnetic precession. Two small coils allow a magnetic field gradient to be applied to the interaction region, with both the field and the gradient directed along the atomic beam axis. When linear polarization is used the gradient has a value of 1.5 G/cm, and when circular polarization is used, the gradient has a value of 3.0 G/cm. A 30 cm focal length lens collects the atomic fluorescence and focuses it onto a photomultiplier tube (PMT) located outside of the vacuum chamber. An interference filter is placed between the lens and the PMT to select the 461 nm fluorescence from the Sr(5s5p $^1P_1$) final state. In some of the experiments a polarizer is also placed between the PMT and the lens to obtain information about the final state alignment. The coordinate system used in this paper is as follows: the z-axis is directed along the atomic beam axis, the x-axis points from the collision region to the PMT, and the y-axis is antiparallel to the laser beam.

III. Vector Correlation Theory

In this section a method of quantifying the alignment results is discussed. The details of this mathematical framework have been given in previous work;[18,22] only the important points will be outlined here. This theory is based on the work of Driessen et al.[23,24] and Alexander et al.[25] First we assume that the final state alignment is not observed. The total observed energy pooling signal resulting from the collision of two aligned atoms (labeled 1 and 2) can be decomposed into so-called fundamental cross sections:

$$I_{\text{obs}} = \sum_{m_1,m_1',m_2,m_2'} \rho_{m_1m_1'}\rho_{m_2m_2'}\sigma_{m_1m_2;m_1'm_2'} \qquad (3)$$

where I_{obs} represents the observed signal, $\rho_{m_1m_1'}$ and $\rho_{m_2m_2'}$ are the density matrices of each of the initial states, and $\sigma_{m_1m_2;m_1'm_2'}$ are the fundamental cross sections. Also m_1, m_2, m_1', and m_2' are magnetic quantum numbers where the quantization axis is the relative velocity vector of the collision. Since all of the collisions within the thermal atomic beam take place by the faster atoms catching up with the slower atoms, the relative velocity vector always points along the atomic beam axis. The fundamental cross sections, $\sigma_{m_1m_2;m_1'm_2'}$, fall into two categories. If $m_1 = m_1'$ and $m_2 = m_2'$, then the cross section is called a conventional cross section, and it is abbreviated $\sigma_{m_1m_2}$. This is simply the collision cross section when an atom in state m_1 collides with an atom in state m_2. If $m_1 \neq m_1'$ and/or $m_2 \neq m_2'$, then $\sigma_{m_1m_2;m_1'm_2'}$ is called a coherence cross section. These coherence cross sections describe the interference between the various initial states when the colliding atoms are initially in a superposition of different magnetic substates. While conventional cross sections are real valued, coherence cross sections are sometimes complex valued. In addition, not all of the cross sections are independent. For example, we expect that $\sigma_{01} = \sigma_{10}$. As shown in Parks et al.,[22] for the case where two atoms with total angular momentum $j = 1$ collide, the alignment effects can be completely described by the following fundamental cross sections:

$$\sigma_{00},\quad \sigma_{10},\quad \sigma_{1-1},\quad \sigma_{11},\quad \sigma_{01;10},\quad \sigma_{1-1;-11},\quad \text{Re}(\sigma_{00;1-1}) \text{ and } \text{Im}(\sigma_{00;1-1}) \qquad (4)$$

Note that the coherence cross sections $\sigma_{01;10}$ and $\sigma_{1-1;-11}$ can be shown to be real valued.[22]

Now consider an actual experimental system. If the excitation laser is linearly polarized along the z-axis then the population of initial states will be created in the $m_j = 0$ state. A magnetic field directed perpendicularly to the z-axis will cause these states to precess. The symmetry axis is defined at any instant to be the axis that, if it is taken to be the quantization axis, the atoms are in an $m_j = 0$ state. The angle between the z-axis and the symmetry axis, β, is given by $\beta = \omega t$. Here ω is the precession frequency and $1/\omega \approx 1$ μs for the magnetic fields used in this experiment. By inserting the appropriate density matrices into eq 3 (both initial states have the same alignment here), we find

$$I(\beta) = a\cos(2\beta) + b\cos(4\beta) + c \qquad (5)$$

where the parameters a, b, and c are

$$a_l = \frac{n}{8}(4\sigma_{00} - 2\sigma_{11} - 2\sigma_{1-1} - 2\sigma_{1-1;-11})$$

$$b_l = \frac{n}{8}\left(\sigma_{00} + \frac{1}{2}\sigma_{11} + \frac{1}{2}\sigma_{1-1} + \frac{1}{2}\sigma_{1-1;-11} - 2\sigma_{01} - 2\sigma_{01;10} + 2\mathrm{Re}\sigma_{00;1-1}\right) \quad (6)$$

$$c_l = \frac{n}{8}\left(3\sigma_{00} + \frac{3}{2}\sigma_{11} + \frac{3}{2}\sigma_{1-1} + \frac{3}{2}\sigma_{1-1;-11} + 2\sigma_{01} + 2\sigma_{01;10} - 2\mathrm{Re}\sigma_{00;1-1}\right)$$

and n is a normalization constant. The subscript l has been appended to the parameters to denote linear polarization. If this experiment is repeated with circular excitation polarization instead of a linearly polarized laser beam, then the symmetry axis is now defined as the axis around which the atoms are in an $m_j = +1$ state. This system is again described by eq 5, but with different parameters:

$$a_c = \frac{n}{8}\left(-\sigma_{00} + \frac{28}{8}\sigma_{11} - \frac{1}{2}\sigma_{1-1} - \frac{1}{2}\sigma_{1-1;-11} - 2\sigma_{10} - 2\sigma_{01;10} - 2\mathrm{Re}\sigma_{00;1-1}\right)$$

$$b_c = \frac{n}{8}\left(\frac{1}{4}\sigma_{00} + \frac{1}{8}\sigma_{11} + \frac{1}{8}\sigma_{1-1} + \frac{1}{8}\sigma_{1-1;-11} - \frac{1}{2}\sigma_{01} - \frac{1}{2}\sigma_{01;10} + \frac{1}{2}\mathrm{Re}\sigma_{00;1-1}\right) \quad (7)$$

$$c_c = \frac{n}{8}\left(\frac{3}{4}\sigma_{00} + \frac{35}{8}\sigma_{11} + \frac{3}{8}\sigma_{1-1} + \frac{3}{8}\sigma_{1-1;-11} + \frac{5}{2}\sigma_{01} + \frac{5}{2}\sigma_{01;10} + \frac{3}{2}\mathrm{Re}\sigma_{00;1-1}\right)$$

where the subscript c denotes circular polarization.

Until this point, the experiments described involve two initial state atoms, both with the same alignment, colliding. In order to study collisions with nonparallel alignments a magnetic field gradient is used. The laser is linearly polarized along the x-axis, and first a spatially uniform magnetic field is directed along the z-axis. This causes the symmetry vectors of the initial states to precess in the x-y plane. Since all of the atoms are precessing at the same rate, the symmetry vectors of the initial state atoms are parallel at all times and the signal is given by

$$I = \frac{1}{2}(\sigma_{1-1} + \sigma_{11} + \sigma_{1-1;-11}) \quad (8)$$

Now a field with a nearly constant gradient is applied, with both the gradient and the fixed field directed along the z-axis. Immediately after the laser pulse, the symmetry vectors of the initial states will be parallel, and the signal is still given by eq 8. But as time progresses, atoms at different locations will precess by different amounts due to the magnetic gradient. Because the collisions occur between atoms which started at different locations along the z-axis, each of the colliding atoms will have a symmetry vector pointing in a different direction (though they are still constrained to lie in the x-y plane). As shown in Parks et al.,[18] the broad velocity distribution of the atomic beam in combination with the magnetic gradient means that the symmetry vectors of the colliding atoms will quickly become randomized. The net effect of this randomization is to destroy the coherence terms in eq 8. Thus at long times where the gradient has had enough time to completely randomize the states, the ratio of the signal with the gradient on to the signal with the gradient off is

$$s_l = (\sigma_{1-1} + \sigma_{11})/(\sigma_{1-1} + \sigma_{1-1;-11} + \sigma_{11}) \quad (9)$$

This can also be done with circularly polarized excitation. In this case the ratio of the signal with the gradient on to the signal with the gradient off is

$$s_c = \left(\frac{1}{8}\sigma_{11} + \frac{1}{4}\sigma_{00} + \frac{1}{8}\sigma_{1-1} + \frac{1}{2}\sigma_{01}\right)\Big/\left[\frac{1}{8}\sigma_{11} + \frac{1}{4}\sigma_{00} + \frac{1}{8}(\sigma_{1-1} + \sigma_{1-1;-11}) + \frac{1}{2}(\sigma_{01} + \sigma_{01;10}) + \frac{1}{2}\mathrm{Re}\sigma_{00;1-1}\right] \quad (10)$$

This description can be extended to include final state alignment. In principle, the density matrix for the final state only needs to be added to eq 3 and the associated indices added to the fundamental cross section. In practice, however, this is a significant complication. The mathematics have been fully worked out in our previous paper[18] and will not be further commented upon in this section, but several results will be used in section V. We close this section by remarking that the equations of this section have described the Ca data extremely well.[18,22]

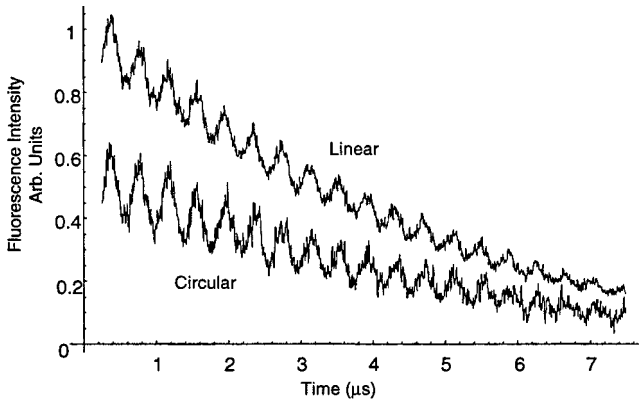

Figure 1. The fluorescence intensity from the final Sr(5s5p $^1P_1$) state plotted as a function of time after the laser pulse excites the initial Sr(5s5p $^3P_1$) state. The modulations with a period of $\approx$0.5 μs result from variations in the energy pooling cross sections as the alignment of the initial state precesses in a magnetic field. The top trace is the signal when linearly polarized excitation is used and the bottom trace is the signal when circularly polarized excitation is used. The two traces were taken on different days, but they have been individually rescaled to reflect the actual relative signal strengths. The magnetic field is directed perpendicular to the relative velocity vector of the collision (the z-azis). In the top trace the laser is linearly polarized along the z-axis, and in the bottom trace the laser is circularly polarized around the axis perpendicular to both the z-axis and the magnetic field.

IV. Effect of Initial State Alignment

In this section, the initial state alignment effect is examined by observing the energy pooling signal without a polarization analyzer. First the initial Sr(5s5p $^1P_1$) state is excited with a linearly polarized laser beam. The laser polarization is directed along the z-axis, and the magnetic field is directed along the x-axis. Thus an aligned population of Sr(5s5p $^1P_1$) states is created, with the symmetry axis parallel to the z-axis immediately after the laser pulse and subsequently precessing around the x-axis. This precession of the initial state alignment will cause a modulation in the energy pooling cross section. This modulation is clearly seen when the final state fluorescence is plotted as a function of time, as in the top trace of Figure 1. The modulation has a total amplitude of just under 10% of the

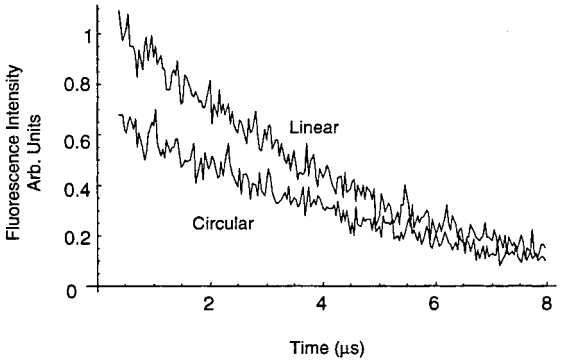

Figure 2. The final state fluorescence intensity as a function of time is plotted as in Figure 1. However, the magnetic field is now directed along the *z*-axis and the laser is polarized along (or around) an axis perpendicular to the *z*-axis. No large modulations are seen because even though the atoms are precessing, they now maintain the same angle with respect to the relative velocity vector of the collision (the *z*-axis).

average linearly polarized signal strength. This modulation is on top of a longer term decay which is the result of the movement of the excited population out of the volume where fluorescence is detected as well as the fluorescence decay of the initial state. This experiment can be repeated with circular polarization. In this case, the laser is circularly polarized around the *y*-axis, and the magnetic field still points along the *x*-axis. Again, the result is that the symmetry vector precesses in the *y*-*z* plane, though it starts out aligned with the *y*-axis. There is again a distinct modulation in the final state fluorescence as seen in the bottom trace in Figure 1. The modulation in the circular case has a total amplitude of about 20% of the average linearly polarized excitation signal strength. In addition, the signal with circular polarization is always smaller than the signal with linearly polarized excitation.

In order to quantify the difference between the signal strength in the linear and circular cases, the magnetic field is directed along the *z*-axis. The laser is first linearly polarized along the *x*-axis, then circularly polarized around the *y*-axis. This means that the symmetry vector remains in the *x*-*y* plane and precesses around the *z*-axis. In this experiment, the laser beam first goes through a polarizer aligned with the *x*-axis and then a Babinet−Soliel compensator. Both linear and circular polarization can be made by adjusting the Babinet−Soliel compensator, allowing the signal in both of these cases to be compared. First linear polarization is produced, and the signal is averaged over 1000 laser pulses. Then circular polarization is made, and the signal is averaged over the same number of laser pulses. This is repeated 15 times. The resulting data is shown in Figure 2. The ratio of linear to circular signal is found to be $r = 1.43 \pm 0.05$. The linear and circular signals shown in Figure 1 were taken under slightly different conditions on different days, and have been rescaled to correctly reflect the actual value for the relative signal strength.

The modulations in the energy pooling cross section are now fit to the form given in section III to obtain the alignment parameters. The long term decay seen in Figure 1 is removed by dividing the signal by a running average with a length equal to one full precession period. The results, after averaging over 10 periods, are shown in Figure 3. The data in this figure have been fit to the form derived in section 3:

$$I(\beta) = a_{l,c}' \cos(2\beta) + b_{l,c}' \cos(4\beta) + 1 \qquad (5')$$

where β is the angle between the symmetry axis of the initial states and the *z*-axis. Also the subscripts *l* and *c* refer to the

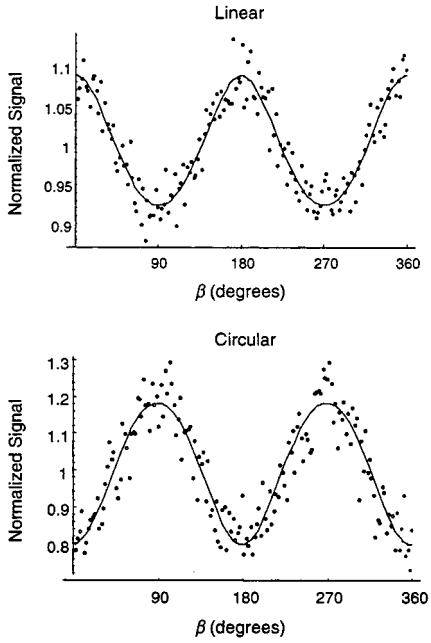

Figure 3. The energy pooling cross section plotted as a function of the angle between the symmetry axis and the *z*-axis as derived from the data in Figure 1. The signal for both the case of linearly polarized excitation and the case of circularly polarized excitation have been normalized so that the average value is 1. The fit is to the form $I(\beta) = a'_{l,c} \cos(2\beta) + b'_{l,c} \cos(4\beta) + 1$.

cases of linear and circular polarization, respectively. The values for the fit parameters are $a_l' = 0.082\ ^{+0.006}_{-0.002}$, $b_l' = 0.006 \pm 0.002$, $a_c' = -0.192\ ^{+0.013}_{-0.006}$, and $b_c' = 0.011 \pm 0.007$.

Next, we discuss the magnetic gradient data. As described in section 3, the symmetry vectors are made to precess in the *x*-*y* plane, and a magnetic gradient destroys the coherence terms. This is seen in Figure 4, where the signal with the gradient on, divided by the signal with the gradient off, is plotted for both linear and circular polarization. Dividing the gradient data by the nongradient data removes the long term decay seen in Figure 1, but it also makes the data look noisy at long times because the two signals that are being compared get small. The clearest gradient effect is seen in the circular case. At $t = 0$ the ratio of the two signals is one, because the gradient has not had time to affect the alignment of the initial states. But as time progresses the signal almost doubles. This indicates that the relevant coherence terms, $\sigma_{01;10}$ and $\mathrm{Re}(\sigma_{00;1-1})$, have large negative values. However in the linear case, the signal does not change much when the gradient is applied. This means that the relevant coherence cross section, $\sigma_{1-1;-11}$, has a small magnitude. The value for the parameters $s_l = 0.96 \pm 0.05$ and $s_c = 1.93 \pm 0.11$, which represent the ratios of the signals with the gradient on to the signal with the gradient off at times long enough so that the gradient has almost completely randomized the alignment, are found by averaging the long time signal between 4 and 6 μs.

The parameters extracted in this section are summarized in Table 1. The uncertainties quoted in this table are increased to include the error due to the $\pm 10°$ error in the magnetic field alignment and the $\pm 5°$ error in the laser polarization alignment. These source errors are discussed more fully in Parks et al.[18,22] Statistical noise is another source of uncertainty. Finally, included in Table 1 is an uncertainty related to the final state alignment. In the case of Ca, the final state alignment is only weakly correlated with the initial state alignment.[18] However, in the case of Sr the situation is not the same. Since all final

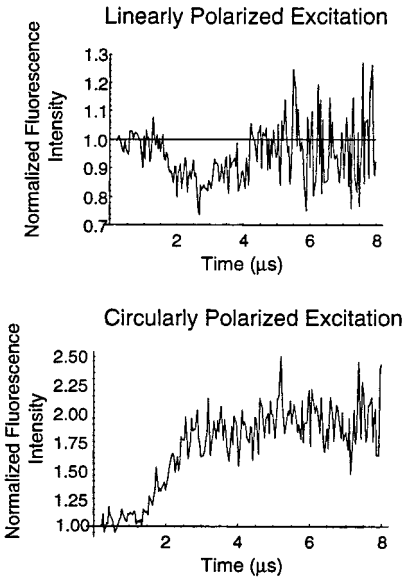

Figure 4. Fluorescence signals versus time, showing the effects of the magnetic field gradient. Here the same geometry as that in Figure 3 is used, with magnetic field directed along the *z*-axis and the laser polarized perpendicular to this. However an additional magnetic field is applied, which is directed along the *z*-axis but has a magnitude that varies approximately linearly along the *z*-axis. As described in the text, this gradient field will destroy any coherence terms that contribute to the cross section after several microseconds. Here the signal with the gradient field turned on divided by the signal with the gradient field turned off is plotted as a function of time.

TABLE 1: Values of the Fit Parameters

parameter	value[a]
a_l'	$0.082^{+0.006}_{-0.020}$
b_l'	$0.006^{+0.002}_{-0.012}$
a_c'	$-0.19^{+0.05}_{-0.01}$
b_c'	$0.011^{+0.007}_{-0.012}$
r^b	1.43 ± 0.05
s_l^c	0.96 ± 0.05
s_c^c	1.93 ± 0.11

[a] The values for the parameters measured in section IV. The modulations resulting from the magnetic precession are fit to the form $I(\beta) = a_{l,c}' \cos(2\beta) + b_{l,c}' \cos(4\beta) + 1$. [b] The parameter r is the ratio of the signal with linearly polarized excitation to circularly polarized excitation at $\beta = 90°$. [c] The parameters s_l and s_c and are the ratio of the signal with the magnetic gradient turned on to the signal with the magnetic gradient switched off for linear and circular excitation, respectively.

states are not detected equally, an error is introduced. The fluorescence from the final p_x state is emitted away from the detector, so only final p_y and p_z states are observed. Thus we are not truly averaging over all final states. This will be discussed further in the next section. Finally, natural isotopic abundance Sr was used in this experiment. This means that 7% of the Sr is in the form of an isotope with nuclear spin $^9/_2$. The nuclear spin will alter the alignment of the electronic state in these atoms. This effect has been ignored here.

The initial state alignment effect for the Sr process eq 1 and the Ca process eq 2 can be completely described with seven parameters, six of which are obtained for both Ca and Sr. The values for these cross sections that were measured in this work are given in Table 2 for both Ca and Sr. The Ca cross sections are averaged over a velocity distribution with a mean of 690 m/s and a full width half maximum of 750 m/s, and the Sr cross sections are averaged over a velocity distribution with a mean of 430 m/s and a fwhm of 460 m/s. There are some striking

TABLE 2: Values for the Fundamental Cross Sections for Ca and Sr Energy Pooling[a]

parameter	Ca[b]	Sr[c]
σ_{00}	$1.14^{+0.02}_{-0.01}$	$1.09^{+0.02}_{-0.04}$
σ_{11}	0.11 ± 0.02	$0.47^{+0.07}_{-0.02}$
σ_{1-1}	1.05 ± 0.15	1.30 ± 0.15
$\sigma_{1-1;-11}$	0.72 ± 0.13	0.07 ± 0.10
σ_{01}	0.34 ± 0.15	1.69 ± 0.19
$\sigma_{01;10}$	-0.07 ± 0.15	-1.01 ± 0.18
$\mathrm{Re}(\sigma_{00;1-1})$	$-0.61^{+0.03}_{-0.02}$	$-0.30^{+0.03}_{-0.02}$

[a] Data in both columns are normalized to $\frac{1}{8}\left(3\sigma_{00} + \frac{3}{2}\sigma_{11} + \frac{3}{2}\sigma_{1-1} + \frac{3}{2}\sigma_{1-1;-11} + 2\sigma_{01} + 2\sigma_{01;10} - 2\,\mathrm{Re}\,\sigma_{00;1-1}\right) = 1$ [b] The Ca cross sections are averaged over a velocity distribution with a mean of 690 m/s and a fwhm of 750 m/s. This data is from Parks et al.[18,22] [c] The Sr cross sections are averaged over a velocity distribution with a mean of 430 m/s and a fwhm of 460 m/s.

differences as well as similarities between the cross sections. In the Ca case the cross section σ_{01} is small, but in the Sr case it is the largest cross section of all. Here σ_{01} is a conventional cross section and is the energy pooling cross section when an $m_j = 0$ state collides with an $m_j = +1$ state. Its associated coherence cross section, $\sigma_{01;10}$, also has a large magnitude for Sr. This cross section represents the contribution to the signal from the interference between an $m_j = 0$ plus $m_j = +1$ and an $m_j = +1$ plus $m_j = 0$ collision. The coherence term $\sigma_{1-1;-11}$, which is large in the Ca case, is very small in the Sr case. There are also similarities. The cross sections σ_{00} and σ_{1-1} are sizable for both systems and σ_{11} is the smallest cross section in both cases, although σ_{11} is larger for Sr than for Ca. Also $\mathrm{Re}(\sigma_{00;1-1})$ is negative in both cases, although it has a larger magnitude for Ca than for Sr.

V. Final State Alignment

The alignment of the final Sr(5s5p $^1P_1$) state is also investigated. The most basic parameter is the behavior of the signal, averaged over the modulations due to the magnetic precession, as the detector polarizer is rotated. Examples of this data are plotted in Figure 5 for both linear and circular excitation. Here the detector polarizer is rotated 180° in 15° steps. Let θ represent the angle between the axis of the detector polarizer and the *z*-axis. The signal is largest when the detector polarizer is parallel to the *z*-axis ($\theta = 0$). When the polarizer is parallel to the *y*-axis ($\theta = 90°$), the signal decreases by 70% in the case of linear excitation and 81% in the circular case. These data are fit to the form[18]

$$I(\theta) = k_{l,c} + l_{l,c} \cos(2\theta) \tag{11}$$

where the two parameters $k_{l,c}$ and $l_{l,c}$ describe the shape of the curve. For the data in Figure 5 the average signal is set equal to 1, thus the quantity obtained from the fit is $l_{l,c}/k_{l,c}$. For the case of linear polarization the amplitude of the modulation is $l_l/k_l = 0.175 \pm 0.012$, and for the case of circular polarization $l_c/k_c = 0.102 \pm 0.020$.

Next we look at how the modulations due to the magnetic precession change as the detector polarizer is rotated. At each value of θ the modulations as the atoms precess in the magnetic field are fit to the form[18]

$$I(t) = p \cos 2\omega t + q \sin 2\omega t + u \cos 4\omega t + v \sin 4\omega t + 1 \tag{12}$$

where the parameters p, q, u, and v depend on θ. This is simply

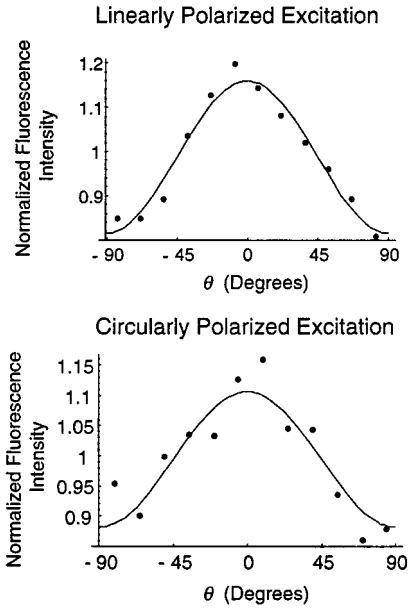

Figure 5. Fluorescence versus detector polarizer angle. A polarizer is placed between the fluorescence detector and the interaction region. Here the signal is averaged over the modulations due to the magnetic precession and plotted as a function of the angle θ between the axis of the polarizer and the z-axis.

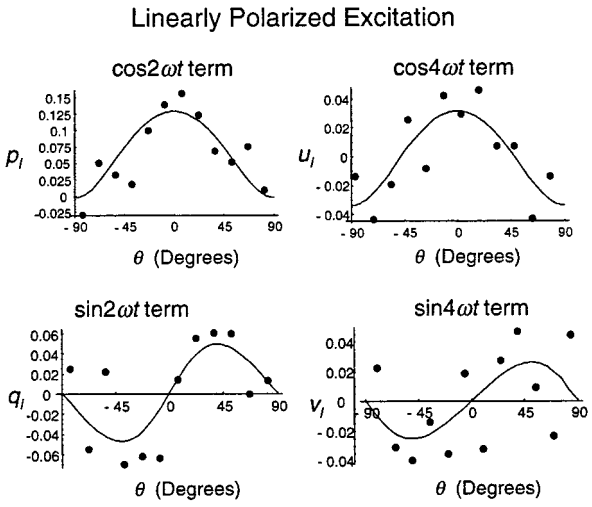

Figure 6. The dependence of the signal modulations due to the precession of the initial state as a function of the detector polarizer angle θ is examined here for the case of linearly polarized excitation. For any particular θ the magnetic precession of the initial state alignment produces modulations in the energy pooling signal which can be fit to the form[18] $I(t) = p_l \cos 2\omega t + q_l \sin 2\omega t + u_l \cos 4\omega t + v_l \sin 4\omega t + 1$. As shown in these plots, the fit parameters p_l, q_l, u_l, and v_l depend on θ.

eq 5 with the sin2ωt and sin4ωt terms added because the symmetry around the z-axis has now been broken. This formula was derived in Parks et al.[18] The parameters p_l, q_l, u_l, and v_l are plotted as a function of θ in Figure 6 for linearly polarized excitation. There appear to be very large modulations in all of these parameters. In Figure 7 the parameters p_c and q_c are plotted for circular polarization. In the circular case the signal is too noisy to see any modulation in the parameters u_c and v_c. An additional problem is that a small amount of the initial state fluorescence from the Sr(5s5p $^3P_1$) → Sr(5s^2 $^1S_0$) transition may have leaked through the interference filter in both the linearly and circularly polarized excitation cases. This is not a problem in the Ca studies, but the initial state fluorescence is 20 times higher here because of the shorter lifetime of the Sr(5s5p $^3P_1$)

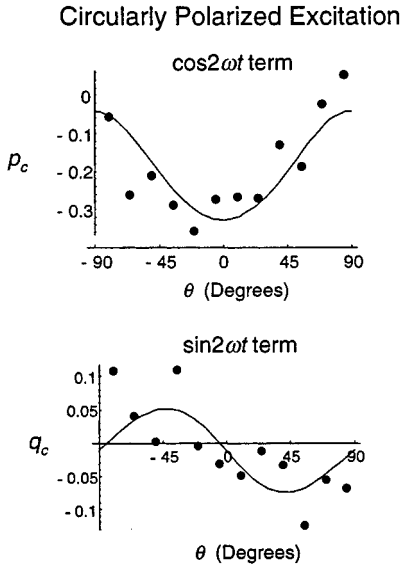

Figure 7. The dependence of the initial state alignment effect is plotted here for the case of circularly polarized excitation. As described in Figure 6, the fit parameters p_c, q_c, u_c, and v_c that describe the modulations resulting from the magnetic precession will depend on the angle between the axis of the detector polarizer, θ, and the z-axis. Only p_c and q_c are plotted here. The scatter in the parameters u_c, and v_c is too large to see any definite trends.

state. As the initial state precesses, this fluorescence is modulated at a frequency of ωt when viewed through the detector polarizer. It is impossible to confirm that the modulations seen in $p_{l,c}$ and $q_{l,c}$ are not an artifact. This problem could easily have been solved by using an additional filter; however, this was not done before the experiment was ended.

There is evidence that some of the final state alignment effect is real. None of the modulation seen in the cos4ωt and the sin4ωt terms can be explained by this artifact. Furthermore, all of the modulation in the cos2ωt and the sin2ωt terms cannot be due to the artifact. To see this, consider the possibility that all of the modulation seen in p_l and q_l is due to the initial state fluorescence leaking through the interference filter. We can then predict what modulation would be seen in p_c and q_c due to the artifact. The initial state fluorescence, as seen by the detector, should be twice as intense when linear polarization is used than when circular polarization is used. This is because in the circular case most of the fluorescence is emitted in the x-y plane away from the detector. Also, the average signal is just over half as strong when circular polarization is used than when linear polarization is used. This means that the modulation in p_l and q_l should be approximately equal to the modulation in p_c and q_c. However, as is seen in Figures 6 and 7 the modulation in p_c and q_c is actually twice that of the modulation in p_l and q_l. Thus, while we cannot accurately measure this final state alignment effect, there is evidence that the modulations in the signal resulting from the magnetic precession are strongly dependent on the angle of the detector polarizer. The modulations in $p_{l,c}$ and $q_{l,c}$ seen in Figures 6 and 7 represent an upper limit on the actual alignment effect.

VI. Discussion

In this paper the alignment effects in the energy pooling process: Sr(5s5p $^3P_1$) + Sr(5s5p $^3P_1$) → Sr(5s5p $^1P_1$) + Sr(5s^2 $^1S_0$) have been presented. In Parks et al. the analogous process in Ca was studied: Ca(4s4p $^3P_1$) + Ca(4s4p $^3P_1$) → Ca(4s4p $^1P_1$) + Ca(4s^2 $^1S_0$).[18,22] In both cases the total energy transfer signal is larger with linearly polarized initial states than with

circularly polarized initial states. The energy pooling cross section depends significantly on the alignment and orientation of these linear or circular states. When the symmetry axes of both atoms are parallel to the *z*-axis the signal is maximum (that is when the atoms are both in an $m_j = 0$ state; the relative velocity vector of the collisions is directed along the *z*-axis). A uniform magnetic field causes these states to precess, and the signal decreases as the symmetry axis is rotated away from the *z*-axis. The alignment modulation is even larger for circularly polarized states. In this case, the signal is minimal when the symmetry axis is parallel to the *z*-axis and increases as the symmetry axis rotates away from the atomic beam axis. These effects are seen for both Ca and Sr, but they are much more pronounced than those for Ca than those for Sr. In the case of Ca, the signal is larger when two p_x states collide than when a p_x and a p_y state collide, but this is not true for that of Sr. This is reflected in the values of $\sigma_{1-1;-11}$ in Table 2.

In this experiment, the final state alignment was also measured. In the case of Ca, the ratio of *y*-polarized fluorescence to *z*-polarized fluorescence was found to be 0.60 ± 0.03. There is a measurable correlation between the final state alignment and the initial state alignment, but this correlation is weak. In the Sr case, the *z*-polarized final state fluorescence also predominates but to a lesser extent. This effect is also different when linear polarization and circular polarization is used. When linearly polarized excitation is used, the ratio of *y*-polarized fluorescence to *z*-polarized fluorescence is 0.70 ± 0.02 and in the circular case it is 0.81 ± 0.03. There is also evidence that the final state alignment is strongly correlated with the initial state alignment but the experiments were unable to accurately measure this.

The exact cause of the differences between the Ca and Sr cases is hard to pin down without a detailed theory of this type of collision, which does not yet exist. A simplistic picture is that when the sum of m_j quantum numbers is zero or one, the energy transfer is relatively efficient. This may be indicative of which potential curves are responsible for the energy transfer. However, it is also possible that multiple crossings occur, since there are many states within a small range of energies. None of the relevant potential curves for the Ca−Ca collision and only a few of the Sr−Sr curves have been published.[26] Even though the structure of Ca and Sr is very similar, it is possible that differences in these potentials could account for the different alignment effects seen in the two atomic systems. Previous theoretical treatments for this type of collision process do not fully take into account spin−orbit coupling. At close separations, the collision complex can be described by molecular states in a basis where the electronic spin and orbital angular momentum are uncoupled. Avoided crossings in this region can probably explain the energy pooling processes observed here. However there is another region at larger interatomic distances where the separation between the different potential curves is comparable to the spin−orbit coupling. The behavior in this region is likely to be quite complicated since at the collision velocities of these experiments there is time for the spin−orbit interaction to significantly mix the populations in the molecular states. The larger spin−orbit coupling of Sr, as well as the slower collision velocity, could account for some of the differences from the Ca data.

In this work we have presented a detailed description of the alignment and orientation effects in the energy pooling process $Sr(5s5p\ ^3P_1) + Sr(5s5p\ ^3P_1) \rightarrow Sr(5s5p\ ^1P_1) + Sr(5s^2\ ^1S_0)$. The effects of initial state alignment, integrating over all final states, are almost completely described here. There are also indications of final state alignment, but it is not thoroughly studied. This, taken with our previous Ca work, provides a quantitative body of work on collisions between two aligned and oriented alkali-earth atoms. In addition, we have demonstrated how magnetic fields can be exploited to obtain a great deal of alignment information. New theoretical techniques will probably be needed to fully model these alignment effects. But the distinct modulations that are observed in the energy pooling cross section hint that there are important general principles waiting to be uncovered.

Acknowledgment. The authors gratefully acknowledge support by the National Science Foundation.

References and Notes

(1) Hertel, I. V.; Schmidt, H.; Bahring, A.; Meyers, E. *Rep. Prog. Phys.* **1985**, *48*, 375.

(2) Campell, E. E. B.; Hertel, I. V. *Adv. Chem. Phys.* **1988**, *72*, 37.

(3) Leone, S. R. *Acc. Chem. Res.* **1992**, *25*, 71.

(4) Kovelenko, L. *The Chemical Dynamics and Kinetics of Small Radicals*; World Scientific: Singapore, 1995; p 730.

(5) Rettner, C. T.; Zare, R. N. *J. Chem. Phys.* **1981**, *75*, 3636.

(6) Rettner, C. T.; Zare, R. N. *J. Chem. Phys.* **1982**, *77*, 2416.

(7) Manders, M. P. I; Driessen, J. P. J.; Beijerinck, H. C. W.; Verhaar, B. J. *Phys. Rev. A* **1988**, *37*, 3237.

(8) Spain, E. M.; Dalberth, M. J.; Kleiber, P. D.; Leone, S. R. *J. Chem. Phys.* **102**, 9532 (1995).

(9) Busser, W.; Neuschafer, D.; Leone, S. R. *J. Chem. Phys.* **1987**, *87*, 3833.

(10) (a) Meijer, H. A. J.; Zeegers, Th.; Pelgrim, T. J. C.; Heideman, H. G. M. *J. Chem. Phys.* **1989**, *90*, 729. (b) Meijer, H. A. J.; Pelgrim, T. J. C.; Heideman, H. G. M.; Morgenstern, R.; Andersen, N. *J. Chem. Phys.* **1989**, *90*, 738.

(11) Kircz, J. G.; Morgenstern, R.; Nienhuis, G. *Phys. Rev. Lett.* **1982**, *48*, 610.

(12) Wang, M.-X.; Keller, J.; Boulmer, J.; Weiner, J. *Phys. Rev. A* **1987**, *35*, 934.

(13) Smith, C. J.; Driessen, J. P. J.; Eno, L.; Leone, S. R. *J. Chem. Phys.* **1982**, *96*, 8212.

(14) Driessen, J. P. J.; Eno, L. *J. Chem. Phys.* **1992**, *97*, 5532.

(15) Collins, T. L. D.; McCaffery, A. J.; Wynn, J. N. *Phys. Rev. Lett.* **1991**, *66*, 137.

(16) Op de Beek, S. S.; Driessen, J. P. J.; Robben, K. H. J. M.; Beijerinck, H. C. W.; Verhaar, B. J. *Phys. Rev. A* **1997**, *56*, 2833.

(17) Mestdagh, J. M.; Visticot, J. P.; Meynadier, P.; Sublemontier, O.; Suits, A. G. *J. Chem. Soc., Faraday Trans.* **1993**, *89*, 1413.

(18) Parks, H. V.; Leone, S. R. *Phys. Rev. A* **1999**. In press.

(19) Neuman, J. A.; Cooper, J.; Gallagher, A. *Phys. Rev. A* **1997**, *56*, 432.

(20) Kelly, J. F.; Harris, M.; Gallagher, A. *Phys. Rev. A* **1988**, *38*, 1225.

(21) Neumann, J. A.; Gallagher, A. *Phys. Rev. A* **1998**, *57*, 2231.

(22) Parks, H. V.; Spain, E. M.; Smedley, J. E.; Leone, S. R. *Phys. Rev. A* **1998**, *58*, 2136.

(23) Driessen, J. P. J.; Eno, L. *J. Chem. Phys.* **1992**, *97*, 5532.

(24) Driessen, J. P. J.; Leone, S. R. *J. Phys. Chem.* **1992**, *96*, 6136.

(25) Alexander, M. H.; Dagdigian, P. J.; DePristo, A. E. *J. Chem. Phys.* **1977**, *66*.

(26) Boutassetta, N.; Allouche, A. R.; Auber-Frecon, M. *Phys. Rev. A* **1996**, *53*, 3845.